Carbon 213 (2023) 118295

Contents lists available at ScienceDirect

Carbon

journal homepage: www.elsevier.com/locate/carbon

Alkali metals induced stacking phase transition of graphite

Xia Wang [a,1], Wenchang Zhang [a,1], Kun Ni [a], Fei Pan [a,**], Yanwu Zhu [a,b,*]

[a] Department of Materials Science and Engineering, School of Chemistry and Materials Science, University of Science and Technology of China, Hefei, Anhui, 230026, China

[b] Key Laboratory of Precision and Intelligent Chemistry, University of Science and Technology of China, Hefei, Anhui, 230026, China

ARTICLE INFO

Keywords:
Graphite
Alkali metal
Rhombohedral phase
Hexagonal phase
Stacking phase transition

ABSTRACT

It is well known that alkali metals can intercalate into graphite to form graphite intercalation compounds but the structural change of graphite induced by alkali metals has been paid less attention. Herein, we report that alkali metals (Li, Na, K) induce the phase transition from ABC-stacking (or 3R phase) to AB-stacking (or 2H phase) of graphite. Specifically, for the graphite powder containing ~45% 3R phase in a mixed phase, the temperature needed to ensure a complete stacking phase transition is 600 °C, 500 °C or 350 °C, for Li, Na or K, respectively, much lower than that needed in bare annealing (1800 °C) while without these alkali metals. Simulations based on density functional theory (DFT) suggest that the charge transfer from alkali metals to graphene distinctly lowers the energy barrier of transition, explaining the different phase transition temperatures for these alkali metals.

1. Introduction

The stacking order of layered materials, through changing the interlayer electron interaction and lattice symmetry, strongly affects the band-structure and the electronic properties [1,2]. In the case of bulk graphite, there are two common periodic stacking configurations: AB-stacking, which is called hexagonal or Bernal phase (or 2H phase), and ABC-stacking, which is called rhombohedral phase (or 3R phase), with each lattice structure illustrated in Fig. 1a [3,4]. It has been shown that 2H phase (ABA-stacking) of trilayer graphene is a semimetal with an electrically tunable band overlap between the valence and conduction bands, whereas 3R phase (ABC-stacking) of trilayer graphene is a semiconductor with an electrically tunable band gap [5–9]. In general, 2H phase in bulk graphite is slightly more stable than 3R phase in thermodynamics [4,7]. The stacking-fault energy in 2H graphite measured by electron transmission microscopy is positive (~0.09 meV per atom) [10,11]; calculations showed that the cohesive energy of 2H graphite exceeds that of 3R graphite by 0.9 meV per atom [12]. More recent calculation gave a stacking-fault energy of ~0.11 meV per atom [13], close to the above measured stacking-fault energy. It was proposed that 3R phase could be converted into 2H phase by high-temperature (above 1025 °C) treatment to overcome the enthalpy difference of 0.59 ± 0.17 kJ mol^{-1}. Another experiment showed that treatment at 1800 °C was necessary to complete this phase transition [14].

For thin graphite films, *e.g.*, trilayer graphene, the energy difference between ABA and ABC stackings has been calculated as 0.18 meV per atom [7], and the experiment showed the ABC trilayer graphene domains on the SiO_2 substrate are stable up to 800 °C [4]. A trilayer graphene containing mixed ABC and ABA domains could be transformed to a film with more ABA domains by evaporating triazine onto the trilayer surface at 150 °C [15]. Thin graphitic films with mixed stackings could be locally transformed to AB-stacking by Joule heating (applied on a ~7.5-nm-thick film) or laser illumination (applied on ~ 2.5-nm-thick film) [16]. In addition, it was reported that the shear force (*i.e.*, the force parallel to the surface) could trigger the transformation from ABC- to AB-stacking when the force is applied along the armchair edge direction of a thin graphite film [17], however the shear force induced effect works only when the graphene is close to the contact area. A potentially scalable method is lacking to realize the transformation of 3R phase to 2H phase in graphite.

* Corresponding author. Department of Materials Science and Engineering, School of Chemistry and Materials Science, University of Science and Technology of China, Hefei, Anhui, 230026, China.

** Corresponding author.

E-mail addresses: wangxia800@mail.ustc.edu.cn (X. Wang), zwc990509@mail.ustc.edu.cn (W. Zhang), nikun@ustc.edu.cn (K. Ni), feipan@ustc.edu.cn (F. Pan), zhuyanwu@ustc.edu.cn (Y. Zhu).

[1] These authors contributed equally to this work.

https://doi.org/10.1016/j.carbon.2023.118295
Received 21 March 2023; Received in revised form 2 July 2023; Accepted 13 July 2023
Available online 13 July 2023
0008-6223/© 2023 Published by Elsevier Ltd.

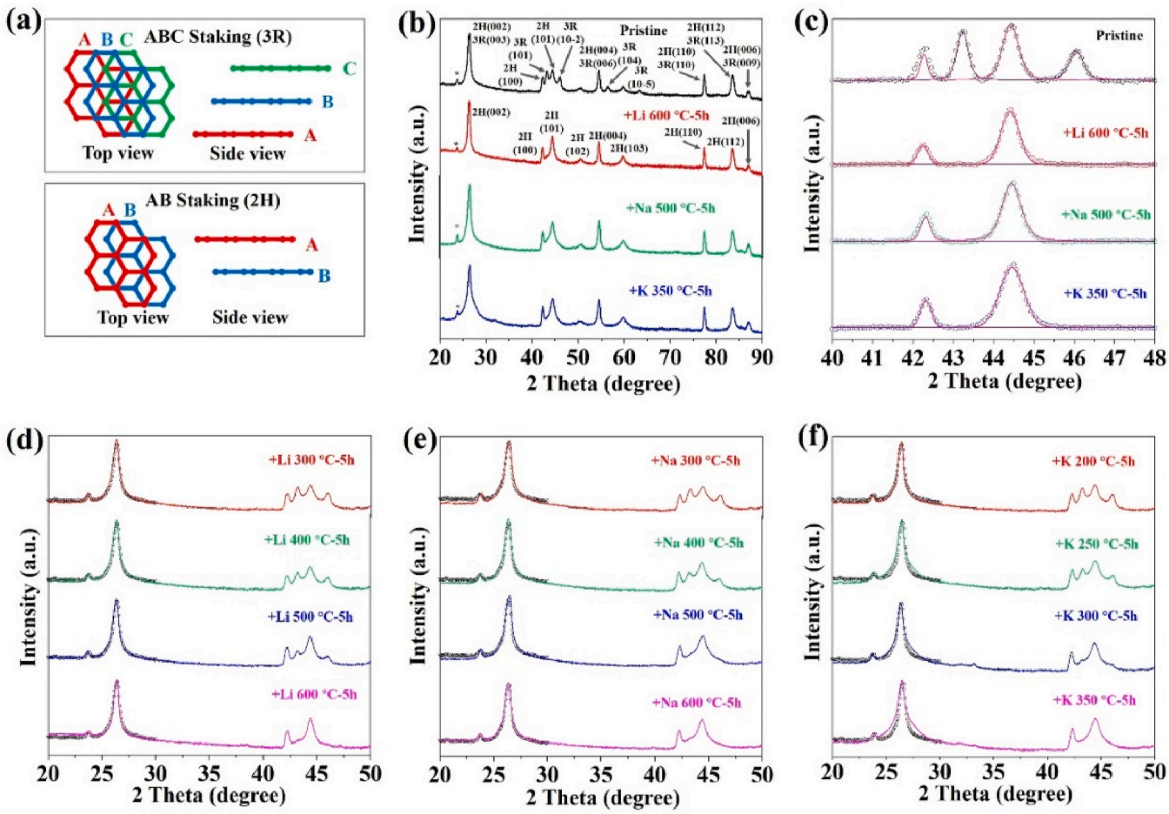

Fig. 1. (a) Schematics of ABC-stacking (3R phase) and AB-stacking (2H phase) graphite. (b) Cu K_α (radiation wavelength $\lambda = 0.15418$ nm) powder XRD patterns of 200 mg graphite before annealing, and after annealing with 40 mg Li at 600 °C for 5h, with 40 mg Na at 500 °C for 5h, or with 40 mg K at 350 °C for 5 h, respectively. Diffraction peaks corresponding to the 2H or 3R phase are indicated by the arrows. Asterisks (*) point to the diffraction peaks originated from Cu K_β (radiation wavelength $\lambda = 0.13922$ nm). (c) Fitting of XRD patterns in the fingerprint range of 40° ~ 48°. The circles indicate experimental data; the pink or purple lines are the simulated lines of 2H or 3R phase. Selected XRD diffraction peaks of (002)/(003) crystal planes for samples obtained by annealing pristine graphite with (d) Li, (e) Na, and (f) K at various temperatures for 5h. Black circles in each figure indicate the same experimental data of pristine graphite to compare with the data from annealed samples. (A colour version of this figure can be viewed online.)

Previously, we have found that the stacking phase transition of 3R phase to 2H phase in graphite powder can be triggered by charge transfer of lithium nitride (α-Li_3N), which improves the repulsion between the layers and reduces the energy transition barrier between the 3R and 2H phases [18]. One puzzle is whether more accessible, pure alkali metals can induce the phase transition. It is well known that potassium (K) can intercalate into interlayers of graphite at temperature of 310–530 °C to form Stage 1 to Stage 4 graphite intercalation compounds (GICs), such as KC_8, KC_{24}, KC_{36} and KC_{48} [19]. Due to the energetic instability of sodium (Na)-GICs [20], however, Na-GICs do not readily form [21]. On the other hand, the reaction of liquid lithium (Li) with graphite is hindered by the difficulty of infiltration [22], thus Li-GICs are only obtained either by immersing graphite in quasi-saturated vapor of Li or by compressing Li with graphite. Stage 1 or Stage 2 Li-GIC was obtained by immersing pyrolytic graphite in pure liquid Li or liquid alloy consisting of 4 wt% Li in Na at 350 °C for 8 h [23]. Compared to the studies on the intercalation into graphite, the structural change of graphite induced by these alkali metals has been paid less attention.

In this work, we find that heating the mixture of graphite with alkali metals (Li, Na and K) can induce the stacking phase transition from 3R to 2H in bulk graphite powder. The critical temperature for a complete phase transition of the 3R phase in graphite powder decreases from 600 °C to 500 °C and 350 °C, for Li, Na and K, due to the enhanced electron injection from alkali metals to graphite. Density functional theory (DFT) simulations have been performed to show the adsorption of alkali metals atoms and charge transfer to ABC-stacking trilayer graphene, which remarkably lowers the phase transition energy barrier to ABA-stacking trilayer graphene.

2. Experimental section

Experiments: Graphite powder with grain size of 400 nm (D50 < 400 nm, 99.95%, metals basis) was purchased from Macklin Inc. (Shanghai, China). Li plates were purchased from Guangdong Canrd New Energy Technology CO., Ltd., China. Na and K chunks were purchased from Sinopharm Chemical Reagent Co., Ltd., China. In a typical experiment, graphite powder and alkali metal were loaded into a quartz tube (length: 150 mm; diameter: 15 mm) in a glovebox at Ar atmosphere. Then the tube was sealed in vacuum, and sample was subsequently heated with a heating rate of 5 °C min^{-1} at Ar atmosphere (flow rate of 100 sccm) in a horizontal tube furnace, followed by annealing at various temperatures for several hours. After annealing, the samples were washed by deionized water and then dried at 80 °C in ambience.

Large area few-layer graphite (FLG) flakes were obtained by mechanical exfoliation of centimeter-size graphite crystals (flaggy graphite, purchased from NGS, Germany) and placed onto a SiO_2/Si substrate (FLG-SiO_2/Si). FLG-SiO_2/Si was annealed in the presence of Li, Na or K chunks (placed next to but not directly contacting to FLG- SiO_2/Si to prevent etching of SiO_2/Si) at 600 °C, 500 °C or 350 °C for 5 h, respectively, to further verify the effect of charge injection.

Characterizations: X-ray diffraction (XRD) was carried out on a high-resolution X-ray diffractometer (Cu K_α radiation with a wavelength of 0.15418 nm, operating at 40 kV and 30 mA, Rigaku SmartLab 3 kW, Japan) with a scan rate of 10° min^{-1}. Data were collected in the range of 5°–90° at a resolution of 0.02°. Raman spectra of graphite were collected with a Raman (Renishaw in Via Raman Micro-scope, UK). The laser wavelength 532 nm, and the diameter of the laser spot is ~1 μm.

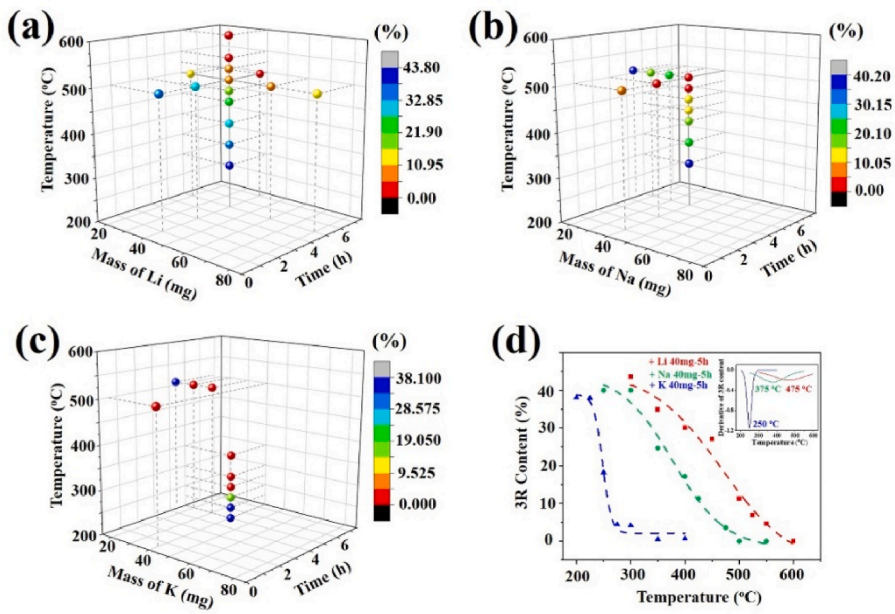

Fig. 2. Calculated content (%) of residue 3R phase by fitting powder XRD patterns of 200 mg graphite powder annealed with various amount of (a) Li, (b) Na or (c) K at various temperatures for different time durations (more details are shown in Table S2). (d) Calculated content (%) of residue 3R phase in graphite powder as a function of temperature after annealing 200 mg graphite with 40 mg alkali metals for 5 h in each annealing. Dashed curves are the fitting of data with the Boltzmann distribution and the differential curves are shown in the inset. (A colour version of this figure can be viewed online.)

Scanning electron microscopy (SEM) images were obtained by a field-emission SEM (Hitachi SU8220, Japan). The X-ray photoelectron spectroscopy (XPS) were performed on an XPS facility with Al K_α radiation ($h\nu = 1486.6$ eV) (Thermo Scientific, ESCALAB 250Xi, US).

Simulation: Quantitative phase analysis (QPA) of XRD data was done by using Reflex code embedded in Materials Studio software. The phase of ideal 2H and 3R graphite was optimized from DFT calculations with optB88-vdW [24] functional. To get a more reliable and repeatable result, the background line of experimental XRD data was removed by Origin software and the XRD data was horizontally moved to make the 2H (101) peak have a good alignment with the calculated peak from the ideal 2H phase. Minor deviations between experiment and simulation may be related to the fact that the Cu K_α radiation ($\lambda = 0.15418$ nm) used in powder XRD consists of Cu $K_{\alpha1}$ ($\lambda = 0.15405$ nm) and Cu $K_{\alpha2}$ ($\lambda = 0.15443$ nm), among which the intensity of the former is about twice as the latter (100 : 49.7). Note that the horizontal movement of the peaks do not have any influence on the intensity of the peak, thus should not introduce extra errors for QPA fitting. The X-ray wavelength is 0.154184 nm with the copper source.

The theoretical calculations were conducted by the Vienna ab initio simulation package (VASP) software [25] based on density functional theory (DFT) [26]. The generalized gradient approximation (GGA) [27] of Pewder-Burke-Ernzerhof (PBE) [28] functional was used to describe exchange-correlation functional. For vdW corrections the DFT-D3 [29, 30] method with Becke-Jonson damping was adopted. A plane-wave cutoff energy was set to be 500 eV and spin unrestricted for all calculations. The energy tolerance for self-consistent field (SCF) is 1×10^{-8} eV and the force tolerance for geometry optimization is 1×10^{-4} eV/Å. An 'all band simultaneous update of orbitals' was selected to be the electronic minimization algorithm and the step width in every ionic relaxation was 0.1 Å. An ABC stacking graphene trilayer model and an ABA stacking graphene trilayer model with 20 Å vacuum layer was used. Single atoms of alkali metal (Li, Na and K) were adsorbed on a three-layered 2×2, 3×3 and 5×5 supercell of graphene. The Brillouin zone was sampled by using $5 \times 5 \times 1$ k-point mesh for all the 2×2 supercell calculation, $4 \times 4 \times 1$ k-point mesh for 3×3 supercell and $2 \times 2 \times 1$ k-point mesh for 5×5 supercell. The minimum energy path (MEPs) was calculated by using climbing-image nudged elastic band (CL-NEB) method [31,32].

3. Results and discussion

Graphite powder with a flake size of 1–5 μm was used in this work, as shown in the scanning electron microscopy (SEM) image (Fig. S1a in the Supporting Information). The XRD pattern of graphite powder before annealing is shown in Fig. 1b (blank line), consisting of the mixed diffraction features of 2H and 3R phases in graphite [33]. 9 peaks for 2H phase and 9 peaks for 3R phase in the range of 5°–90° are consistent with the previous report [33]. 4 diffraction peaks (originated from crystal planes of (101), (10–2), (104) and (10–5) in the 3R phase, Fig. 1b) are not overlapped with those of 2H phase and thus used to distinguish the crystal structure. Li foils (thickness: about 448 μm) were stored in a glovebox at argon (Ar) atmosphere; Na and K bulks were stored in liquid kerosene in the glovebox and used after wiping out the kerosene and slicing to small chunks. In a typical experiment, 200 mg of graphite powder and 40 mg of alkali metals (Li, Na, K) were mixed in a quartz tube in the glovebox at Ar atmosphere and then sealed in vacuum, followed by annealing at different temperatures (600 °C, 500 °C, or 350 °C) in a tube furnace for 5 h. After annealing, graphite powder samples were washed by deionized water and then dried at 80 °C in ambience.

After annealing with alkali metals, graphite samples maintain the flake shape with sizes close to those of pristine samples, as shown in SEM images (Figs. S1b, c, d). However, the characteristic diffraction peaks of the 3R phase in XRD patterns of all three graphite powder samples disappear, as seen from Fig. 1b. At the same time, the intensities of diffraction peaks for 2H phase (*e.g.*, those corresponding to (101), (102), and (103) crystal planes) are enhanced, indicating the improved crystallinity of 2H phase. As a control, the XRD of graphite powder after annealing under the same conditions yet without these metals showed no significant changes (Fig. S2). Meanwhile, we did not see any significant changes in the peaks of G band and 2D band in Raman spectra (Fig. S3) or X-ray photoelectron spectroscopy (XPS) C1s spectra (Fig. S4). No significant signals of Li 1s, Na 1s and K 2p were detected in XPS of annealed samples. The atomic ratio (Table S1) remains similar after annealing. Annealing two other graphite powders (Aladdin Industrial Corporation, Shanghai, China) with flake sizes of 5–15 μm and 10–50 μm also gives the similar results, as shown in Fig. S5.

To evaluate the content of 3R phase in graphite powder, fitting of powder XRD patterns in the fingerprint range of 40°–48° (covering 2H (100)/2H (101) and 3R (101)/3R (10–2) diffraction peaks) [34] was performed for all samples, as shown in Fig. 1c. Assuming that all

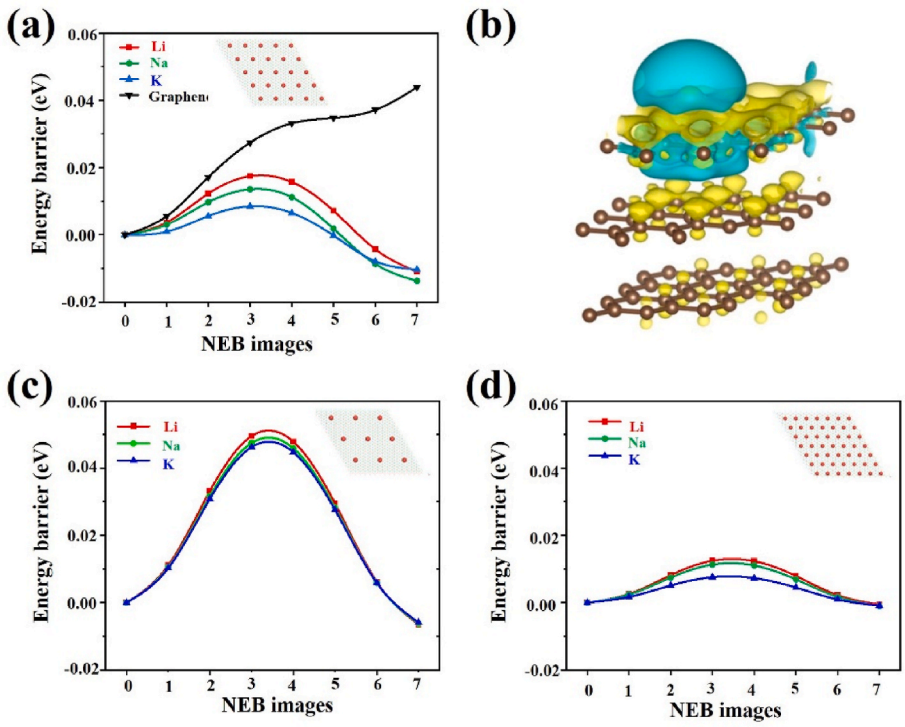

Fig. 3. (a) Nudged elastic band path for trilayer graphene from ABC-stacking to ABA-stacking of pristine and after an alkali metal atom adsorbed on a ABC-stacking trilayer graphene supercell with 33.33% adsorption coverage; (b) Charge density difference of Li atom adsorbed on a 3 × 3 trilayer graphene supercell, where the iso-surface value is 0.0005 e^{-} $bohr^{-3}$; (c) Nudged elastic band path after an alkali metal atom adsorbed on a trilayer graphene supercell with 12% adsorption coverage and (d) a trilayer graphene supercell with 75% adsorption coverage. Insets in (a), (c) and (d) show the corresponding models of alkali metal atoms adsorbed on an ABC stacking trilayer graphene with the same area of ~13.7 nm^2. (A colour version of this figure can be viewed online.)

graphite samples contain only 3R and 2H phases, the calculated content of 3R phase in pristine graphite was 45.15% and then reduced to essentially 0 after annealing with Li (at 600 °C), Na (at 500 °C), and K (at 350 °C) for 5h. As shown in Fig. 1d, e and 1f, after annealing with Li, Na or K, the intensities of diffraction peaks of (101) and (10–2) crystal planes gradually decrease with the temperature till it completely disappears, indicating the transition of 3R phase into 2H phase. The temperature needed for a complete phase transition under the experimental conditions used in this work, is ~600 °C for Li, ~500 °C for Na and ~350 °C for K. To verify if the alkali metal (Li, Na, K) atoms intercalate into the interlayers of graphite after annealing, the XRD peak of (002)/(003) crystal plane (*i.e.*, 20°–30°) of annealed samples were also compared with that of pristine graphite powder. The positions and intensities of diffraction peaks of (002)/(003) crystal planes were coincident with those of pristine graphite, indicating that the interlayers of graphite were not intercalated by Li, Na and K. It also should be mentioned that the intensities and widths of diffraction peaks of (002)/(003) crystal planes of graphite annealing with alkali metals does not change before and after washing by water, as shown in Fig. S6.

In addition, Raman spectroscopy may be used to distinguish the different stackings, but we have not observed the difference in Raman spectra between original graphite and processed graphite described above, probably due to the complicated distribution of stackings in bulk graphite powders. However, Raman spectra of large area FLG flakes have indicated that some ABC stacking regions are transformed to AB stacking, as shown in Fig. S7, evidenced by the changed Raman 2D band after annealing. Na and K caused severe etching of FLG flakes on SiO_2/Si and no samples were left after annealing (Fig. S7a). More research might be carried out to identify the phase transition of large area FLG flakes, which clearly show the transition conditions different from graphite powders.

To further investigate the difference of Li, Na or K on the phase transition from ABC-stacking to AB-staking of graphite, a series of comparative experiments were performed, including the change of annealing temperature and time, mass of alkali metals. When the mass of graphite powder and alkali metals are fixed as 200 mg and 40 mg, the annealing temperature as 350 °C, and the annealing time as 5 h, the content of residue 3R phase is reduced to 34.91% after annealing with Li, to 24.67% with Na and essentially to 0 with K, as shown in Fig. 2, Fig. S8 and Table S2. When the mass of graphite powder and alkali metals are fixed as 200 mg and 40 mg, and the annealing temperature as 500 °C, the content of residue 3R phase is reduced to 4.27% after annealing with Li for 7 h, to 4.59% after annealing with Na for 3 h and essentially to 0 after annealing with K for 0.5 h. When the mass of graphite powder is fixed as 200 mg, and the annealing temperature as 500 °C, and the annealing time as 5 h, the content of residue 3R phase is reduced to 11.8% after annealing with 80 mg Li, essentially to 0 after annealing with 40 mg Na or after annealing with 20 mg K. Fig. 2d further plots the 3R content as a function of annealing temperature for fixed annealing time and graphite/metals mass for each metal, in which the Boltzmann fitting is taken to guide the eyes. From the fittings and the corresponding differential curves shown in the inset, we can clearly see that K brings about the lowest threshold temperature at ~250 °C for the phase transition. From the comparison, we can see that the ability to induce the stacking phase transition follows the order of K > Na > Li, consistent with the work function order of K (2.3 eV), Na (2.75 eV), Li (2.9 eV) [35]. Other factors such as the saturated vapor pressure [36], which may affect the diffusion of metallic vapor into the graphite powder, could also play roles in the phase transition.

To have the hint on the effect of electronic properties of alkali metals on the phase transition, DFT simulations were conducted. In observation of complexity of bulk graphite structure for the simulations (*e.g.*, at least 6-layer unit cell or too many possible slipping reaction pathways), an ABC-stacking trilayer graphene and an ABA-stacking trilayer graphene were used to represent 3R and 2H phases, respectively. Adsorption of single atoms of Li, Na or K on the ABC-stacking trilayer graphene was considered and the transition from ABC- to ABA-stacking achieved by sliding the bottom layer of ABC-stacking trilayer graphene. A climbing-image nudged elastic band (CL-NEB) method was used to obtain the minimum energy paths for the sliding.

Fig. 3a shows the phase transition route from ABC- to ABA-stacking in a supercell model with 33.33% coverage (assuming a metal/carbon atomic ratio of 1:6 as 100% coverage, as for the situation of LiC_6) of alkali metals. From the curves we can see that the adsorption of Li, Na or

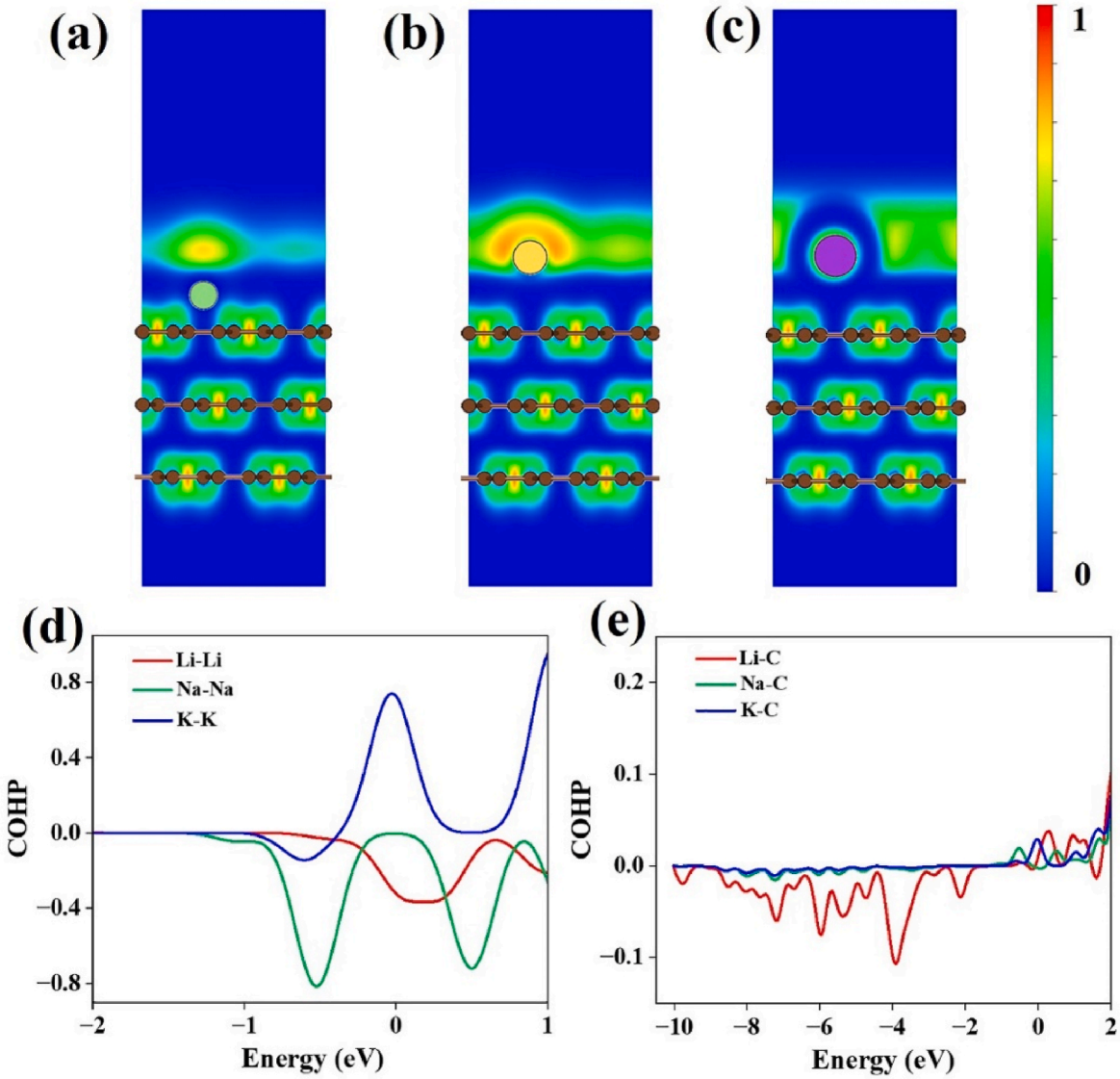

Fig. 4. Electron localization function analysis for (a) Li, (b) Na and (c) K in 2 × 2 supercell with slice direction of (110). Crystal orbital Hamilton population for (d) metal-metal atoms interaction and (e) metal-carbon atoms interaction in 2 × 2 supercell. (A colour version of this figure can be viewed online.)

K can surely reduce the energy barrier in the transition, which is raised by the high energy status of A-A layer stacking during transition. Again, the adsorption of K shows the highest efficiency to reduce the energy barrier (9.24 meV per atom), compared to Na (11.8 meV per atom) and Li (16.4 meV per atom). The charge density difference for the same coverage of Li, Na or K atom adsorbed on a trilayer graphene is shown in Fig. 3b and S9, indicating that the charge transfer mainly occurs between the alkali atoms and the contact layer of trilayer graphene while electrons can also inject into two bottom layers due to the charge transfer between adjacent graphene layers. In addition, the transition energy barriers for 12% and 75% adsorption coverage were also calculated and are shown in Fig. 3c and d. Combing the Bader charge calculations shown in Table S3, we can see the same trend of energy barrier change for 12% and 75% coverage as those in 33.33% coverage for different metals. For the same metal adsorption, the energy barrier decreases as the coverage density increases and the higher coverage would induce less charge transfer between alkali atoms and graphene due to stronger metal-metal interaction.

To have a more detailed description of the states of metal atoms on graphene, we have conducted electron localization function (ELF) analysis, which outputs a value between 0 and 1, where 0 represents a total delocalized electronic property, often related to ionic states, 0.5 represents a free electron state, often related to metallic states, and 1 represents a total localized electronic state, often related to chemical bonds or localized surface or defect states [37]. As we can see, at high metal atom coverage, *e.g.*, in 2 × 2 supercell in FIGs. 4a, b and 4c, all three models show a horizontal metal-metal interaction with ELF value of about 0.35–0.77, indicating that there is a quasi-metallic electron cloud in the metal atom layer. Going to details, Li and Na atoms have a cap-like localized electron states in the opposite side towards graphene layers, while the K atom is more ionic. When the coverage is lower, *e.g.*, in 3 × 3 supercell as shown in Fig. S10, the Li atom shows a fully ionic electronic state, due to the relatively small size. While the Na and K atoms still show metal-metal interactions in this model, with a strong localized surface state on Na atom, and a relatively weak localized surface state on K atom. When the coverage is sufficiently low, *e.g.*, in 5 × 5 supercell, all three types of alkali atoms show ionic property, as shown in Fig. S11.

Crystal orbital Hamilton population (COHP) calculations were conducted to show the interaction between metallic atoms or between metal and graphene [38]. The COHP of metal-metal interactions with different coverage are shown in Fig. 4d and Fig. S12. We can find that there is a

strong bonding interaction of Li–Li and Na–Na in 2 × 2 supercell model while the K–K interaction is anti-bonding, due to the columbic repulsion between electrons in K, which has a larger ionic size. The metal-metal interaction turns to be weaker in 3 × 3 supercell with all three types of alkali atoms have bonding interaction, then disappears in 5 × 5 supercell model. The interaction between metal atom and graphene is also considered, with selecting a carbon atom in the adsorbing hexagonal ring, as shown in Fig. 4e and Fig. S13. We can see that the bonding state of Li–C interaction is stronger than Na–C and K–C interaction. The Li–C interaction decreases while the Na–C and K–C maintains the similar strength with the decreasing coverage. For high coverage model, *e.g.*, in 2 × 2 supercell as shown in Fig. 4e, the anti-bonding interaction of metal-graphene nearby fermi level is noticed, suggesting a weak interaction between metal and graphene. The relationship between metal atoms coverage and the amount of charge transfer are shown in Fig. S14 and Table S4. At low coverage, the charge transfer for all the three metals decreases linearly as the atom coverage lowers. As the coverage increases, the charge transfer deviates from the linear relationship. More research might be carried out to obtain a clearer understanding of the charge transfer from alkali atoms to graphene.

4. Conclusions

In summary, the stacking phase transition from ABC- to AB-stacking in graphite has been induced by alkali metals (Li, Na, K). For the graphite powder containing mixed 3R and 2H phases, the critical temperature needed to ensure the complete phase transition of the 3R phase is ~600 °C, ~500 °C or ~350 °C, for Li, Na or K, respectively. We show that the reduction of energy barriers is attributed to the charge transfer from alkali atoms to graphene, resulting in the reduction of phase transition temperature. Among three metals, K shows the highest efficiency, followed by Na and Li. Our work provides a potentially scalable method to tune the fine structure of graphite.

CRediT authorship contribution statement

Xia Wang: Conception, Conceptualization, material preparation and characterizations, data analysis, Data curation, Formal analysis, manuscript writing and revisions, Writing – original draft. **Wenchang Zhang:** Simulations, data analysis, Data curation, Formal analysis, manuscript writing and revisions, Writing – original draft. **Kun Ni:** Simulations, data analysis, Data curation, Formal analysis, manuscript revisions. **Fei Pan:** Conception, Conceptualization, manuscript writing, Writing – original draft, revisions and, Supervision. **Yanwu Zhu:** Conception, Conceptualization, manuscript writing and revisions, Writing – original draft, and, Supervision.

Declaration of competing interest

The authors declare that they have no known competing financial interests or personal relationships that could have appeared to influence the work reported in this paper.

Acknowledgements

This work was supported by National Key R&D Program of China (Grant No. 2020YFA0711502), Natural Science Foundation of China (Grant Nos. 51972299, 52003265, 52202052, 52273234, 52273239). F. P. is supported by Xiaomi Young Talents Program.

Appendix A. Supplementary data

Supplementary data to this article can be found online at https://doi.org/10.1016/j.carbon.2023.118295.

References

[1] L. Jiang, S. Wang, Z. Shi, C. Jin, M.I.B. Utama, S. Zhao, Y.R. Shen, H.J. Gao, G. Zhang, F. Wang, Manipulation of domain-wall solitons in bi- and trilayer graphene, Nat. Nanotechnol. 13 (2018) 204–208.
[2] J. Zhang, J. Han, G. Peng, X. Yang, X. Yuan, Y. Li, J. Chen, W. Xu, K. Liu, Z. Zhu, W. Cao, Z. Han, J. Dai, M. Zhu, S. Qin, K.S. Novoselov, Light-induced irreversible structural phase transition in trilayer graphene, Light Sci. Appl. 9 (2020) 174.
[3] J.H. Warner, M. Mukai, A.I. Kirkland, Atomic structure of ABC rhombohedral stacked trilayer graphene, ACS Nano 6 (2012) 5680–5686.
[4] C.H. Lui, Z. Li, Z. Chen, P.V. Klimov, L.E. Brus, T.F. Heinz, Imaging stacking order in few-layer graphene, Nano Lett. 11 (2011) 164–169.
[5] C.H. Lui, Z. Li, K.F. Mak, E. Cappelluti, T.F. Heinz, Observation of an electrically tunable band gap in trilayer graphene, Nat. Phys. 7 (2011) 944–947.
[6] W. Bao, L. Jing, J. Velasco, Y. Lee, G. Liu, D. Tran, B. Standley, M. Aykol, S. B. Cronin, D. Smirnov, M. Koshino, E. McCann, M. Bockrath, C.N. Lau, Stacking-dependent band gap and quantum transport in trilayer graphene, Nat. Phys. 7 (2011) 948–952.
[7] M. Aoki, H. Amawashi, Dependence of band structures on stacking and field in layered graphene, Solid State Commun. 142 (2007) 123–127.
[8] K. Zou, F. Zhang, C. Clapp, A.H. MacDonald, J. Zhu, Transport studies of dual-gated ABC and ABA trilayer graphene: band gap opening and band structure tuning in very large perpendicular electric fields, Nano Lett. 13 (2013) 369–373.
[9] M.F. Craciun, S. Russo, M. Yamamoto, J.B. Oostinga, A.F. Morpurgo, S. Tarucha, Trilayer graphene is a semimetal with a gate-tunable band overlap, Nat. Nanotechnol. 4 (2009) 383–388.
[10] C.S.G. Cousins, Elasticity of carbon allotropes. IV. Rhombohedral graphite: elasticity, zone-center optic modes, and phase transformation using transferred Keating parameters, Phys. Rev. B 67 (2003), 024110.
[11] C. Baker, Y. Chou, A. Kelly, The stacking-fault energy of graphite, Philos. Mag. A 6 (1961) 1305–1308.
[12] J. Furthmüller, J. Hafner, G. Kresse, Ab initio calculation of the structural and electronic properties of carbon and boron nitride using ultrasoft pseudopotentials, Phys. Rev. B 50 (1994) 15606–15622.
[13] J.-C. Charlier, X. Gonze, J.-P. Michenaud, First-principles study of the stacking effect on the electronic properties of graphite(s), Carbon 32 (1994) 289–299.
[14] E. Matuyama, Rate of transformation of rhombohedral graphite at high temperature, Nature 178 (1956) 1459–1460.
[15] W. Zhang, J. Yan, C.H. Chen, L. Lei, J.L. Kuo, Z. Shen, L.J. Li, Molecular adsorption induces the transformation of rhombohedral- to Bernal-stacking order in trilayer graphene, Nat. Commun. 4 (2013) 2074.
[16] T. Latychevskaia, S.-K. Son, Y. Yang, D. Chancellor, M. Brown, S. Ozdemir, I. Madan, G. Berruto, F. Carbone, A. Mishchenko, Stacking transition in rhombohedral graphite, Front. Physiol. 14 (2019), 13608.
[17] Y. Yang, Y.-C. Zou, C.R. Woods, Y. Shi, J. Yin, S. Xu, S. Ozdemir, T. Taniguchi, K. Watanabe, A.K. Geim, K.S. Novoselov, S.J. Haigh, A. Mishchenko, Stacking order in graphite films controlled by van der waals technology, Nano Lett. 19 (2019) 8526–8532.
[18] F. Pan, K. Ni, Y. Ma, H. Wu, X. Tang, J. Xiong, Y. Yang, C. Ye, H. Yuan, M.L. Lin, J. Dai, M. Zhu, P.H. Tan, Y. Zhu, K.S. Novoselov, Phase-changing in graphite assisted by interface charge injection, Nano Lett. 21 (2021) 5648–5654.
[19] D.E. Nixon, G.S. Parry, Formation and structure of the potassium graphites, J. Phys. D Appl. Phys. 1 (1968) 291–299.
[20] K. Nobuhara, H. Nakayama, S. Nakanishi, H. Iba, First-principles study of alkali metal-graphite intercalation compounds, J. Power Sources (2013) 585–587.
[21] D.P. DiVincenzo, E.J. Mele, Cohesion and structure in stage-1 graphite intercalation compounds, Phys. Rev. B 32 (1985) 2538–2553.
[22] D. Guerard, A. Herold, Intercalation of lithium into graphite and other carbons, Carbon 13 (1975) 337–345.
[23] S. Basu, C. Zeller, P.J. Flanders, C.D. Fuerst, W.D. Johnson, J.E. Fischer, Synthesis and properties of lithium-graphite intercalation compounds, Mater. Sci. Eng. 38 (1979) 275–283.
[24] J. Klimeš, D.R. Bowler, A. Michaelides, Chemical accuracy for the van der Waals density functional, J. Phys. Condens. Matter 22 (2010), 022201.
[25] G. Kresse, J. Furthmuller, Efficient iterative schemes for ab initio total-energy calculations using a plane-wave basis set, Phys. Rev. B 54 (1996) 11169–11186.
[26] G. Kresse, D. Joubert, From ultrasoft pseudopotentials to the projector augmented-wave method, Phys. Rev. B 59 (1999) 1758–1775.
[27] J.P. Perdew, K. Burke, Y. Wang, Generalized gradient approximation for the exchange-correlation hole of a many-electron system, Phys. Rev. B 54 (1996) 16533–16539.
[28] J.P. Perdew, K. Burke, M. Ernzerhof, Generalized gradient approximation made simple, Phys. Rev. Lett. 77 (1996) 3865–3868.
[29] S. Grimme, J. Antony, S. Ehrlich, H. Krieg, A consistent and accurate ab initio parametrization of density functional dispersion correction (DFT-D) for the 94 elements H-Pu, J. Chem. Phys. 132 (2010), 154104.
[30] S. Grimme, S. Ehrlich, L. Goerigk, Effect of the damping function in dispersion corrected density functional theory, J. Comput. Chem. 32 (2011) 1456–1465.
[31] G. Henkelman, B.P. Uberuaga, H. Jónsson, A climbing image nudged elastic band method for finding saddle points and minimum energy paths, J. Chem. Phys. 113 (2000) 9901–9904.
[32] G. Henkelman, H. Jónsson, Improved tangent estimate in the nudged elastic band method for finding minimum energy paths and saddle points, J. Chem. Phys. 113 (2000) 9978–9985.

[33] M.S. Seehra, U.K. Geddam, D. Schwegler-Berry, A.B. Stefaniak, Detection and quantification of 2H and 3R phases in commercial graphene-based materials, Carbon 95 (2015) 818–823.
[34] K. Guerin, A. Fevrier-bouvier, S. Flandrois, M. Couzi, B. Simon, P. Biensan, Effect of graphite crystal structure on lithium electrochemical intercalation, J. Electrochem. Soc. 146 (1999) 3660–3665.
[35] H.B. Michaelson, The work function of the elements and its periodicity, J. Appl. Phys. 48 (1977) 4729–4733.
[36] A.R. Gordon, The free energies and vapor pressures of the alkali metals, J. Chem. Phys. 4 (1936) 100–102.
[37] B. Silvi, A. Savin, Classification of chemical bonds based on topological analysis of electron localization functions, Nature 371 (1994) 683–686.
[38] R. Dronskowski, P.E. Blochl, Crystal Orbital Hamilton Populations (COHP). Energy-resolved visualization of chemical bonding in solids based on density-functional calculations, J. Phys. Chem. 97 (1993) 8617–8624.